Radical Reactions

International Edition: DOI: 10.1002/anie.201508922
German Edition: DOI: 10.1002/ange.201508922

Bent Carbon Surface Moieties as Active Sites on Carbon Catalysts for Phosgene Synthesis

Navneet K. Gupta, Anastasia Pashigreva, Evgeny A. Pidko, Emiel J. M. Hensen, Leslaw Mleczko, Stefan Roggan,* Erika E. Ember,* and Johannes A. Lercher**

Abstract: *Active sites in carbon-catalyzed phosgene synthesis from gaseous CO and Cl_2 have been identified using C_{60} fullerene as a model catalyst. The carbon atoms distorted from sp^2 coordination in non-planar carbon units are concluded to generate active Cl_2. Experiments and density functional theory calculations indicate the formation of a surface-bound $[C_{60}\cdots Cl_2]$ chlorine species with radical character as key intermediate during phosgene formation. It reacts rapidly with physisorbed CO in a two-step Eley–Rideal-type mechanism.*

The synthesis of phosgene ($COCl_2$) by a catalyzed reaction between gaseous chlorine (Cl_2) and carbon monoxide (CO) is one of the oldest, most reliable, and efficient large-scale chemical processes.[1] Since catalytic $COCl_2$ synthesis has replaced earlier processes based on photolysis,[2] the activated carbon used as catalyst has remained basically unchanged. While several kinetic studies on phosgene formation have been reported,[3] mechanistic insight into carbon-catalyzed $COCl_2$ synthesis and the associated active sites is largely lacking.[4] This may in part be associated with the diversity and chemical complexity of carbon surface structures rendering the identification of the active sites on carbon catalysts highly challenging.

To initiate the development of a new generation of stable and highly active catalysts, the nature of active sites and of the elementary steps of $COCl_2$ synthesis from CO and Cl_2 on activated carbon have been studied. Insight is critical not only to optimize catalytic properties by maximizing the concentration of active sites, but also to minimize production of chlorinated side products.

In a first step, transmission electron microscopy has been used to exemplify the characteristic features of a typical activated carbon catalyst, that is, the ample presence of bent carbon layers, semi-spheres, and carbon cages (Figure 1). Bending of the carbon structures is usually induced by the presence of 5-membered rings or the combination of 5- and 7-membered rings (Stone–Wales defects).[5]

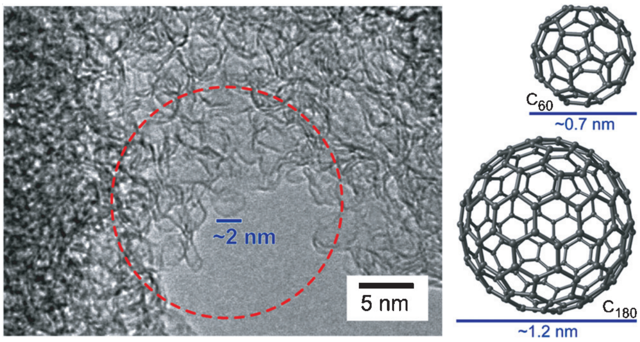

Figure 1. HR-TEM image of an activated carbon catalyst for $COCl_2$ synthesis from CO and Cl_2 showing curled carbon layers (left) and carbon semi-spheres that resemble fullerene-type structures (right).

The diameters of these bent structural units (Figure 1, blue bar) approximate the diameter of fullerenes, which range from 0.71 (C_{60}) to 1.2 nm (C_{176}).[6,7] The structural analogy between the curved surfaces of activated carbon and the molecular structure of fullerenes stimulated us, in consequence, to select fullerenes as well-defined model catalysts. These models lack defect sites, edges, and functional groups. It allows the mechanism of carbon-catalyzed Cl_2 activation and conversion with CO to be explored in the absence of various more reactive but less defined carbon species.

Table 1 compares DFT-computed reaction energies for $COCl_2$ formation and the Cl_2 addition to unsaturated moieties in several model structures with distinct structural characteristics, that is, a planar $C_{32}H_{14}$ graphene model, 2-butene, and C_{60}. Only in the case of C_{60}, the reaction energy is lower than that of the reaction of Cl_2 with CO. The reaction of Cl_2 with graphene is highly endothermic, and addition to graphene has not been observed.[8] Chlorination of butene is strongly exothermic, suggesting the formation of strong and stable C−Cl bonds. We hypothesize, therefore, that the curved structure of the conjugated fullerene π-system provides the appropriate balance between the loss of conjugation energy

[*] N. K. Gupta, Dr. A. Pashigreva, Dr. E. E. Ember, Prof. J. A. Lercher
Technische Universität München, Department of Chemistry and Catalysis Research Center
Lichtenbergstrasse 4, 85748 Garching (Germany)
E-mail: erika.ember@mytum.de
johannes.lercher@ch.tum.de
Dr. E. A. Pidko, Prof. E. J. M. Hensen
Laboratory of Inorganic Materials Chemistry, Schuit Institute of Catalysis, Eindhoven University of Technology
PO Box 513, 5600 MB Eindhoven (The Netherlands)
Dr. E. A. Pidko
Institute for Complex Molecular Systems
Eindhoven University of Technology
PO Box 513, 5600 MB Eindhoven (The Netherlands)
E-mail: e.a.pidko@tue.nl
Prof. L. Mleczko, Dr. S. Roggan
Technology Development, Bayer Technology Services GmbH
51368 Leverkusen (Germany)
E-mail: stefan.roggan@bayer.com

Supporting information and ORCHID(s) from the author(s) for this article are available on the WWW under http://dx.doi.org/10.1002/anie.201508922.

Table 1: DFT-computed reaction enthalpies (B3LYP-D3/TZVP//6-31G-(d,p)) of Cl_2 addition via $X+Cl_2 \rightarrow XCl_2$.

X	Graphene[a]	C_{60}	CO[b]	2-Butene[b]
ΔH_r [kJ mol^{-1}]	+227	−18	−124	−189

[a] The structure of graphene was approximated by a $C_{32}H_{14}$ fragment in this calculation (see the Supporting Information for further details). [b] The experimental ΔH_r values for CO and 2-butene chlorination are −109.6 and −191.2 kJ mol^{-1}, respectively.[1e]

and the energy gain in reactive coordination of Cl_2 (Supporting Information, Figure S1), in line with the relatively low exothermicity of Cl_2 addition to C_{60}.

To test the suitability of C_{60} as a model catalyst for $COCl_2$ synthesis, the material was exposed to CO and Cl_2 pulses at 200 °C (Supporting Information, Figure S2). Once the reversible adsorption of Cl_2 was established, the stable catalytic formation of $COCl_2$ was detected by online mass-spectrometry ($m/z = 63$, Figure 2a), corresponding to $[COCl]^{+\bullet}$. Without catalyst, only negligible concentrations of $COCl_2$ formed (Figure 2b).

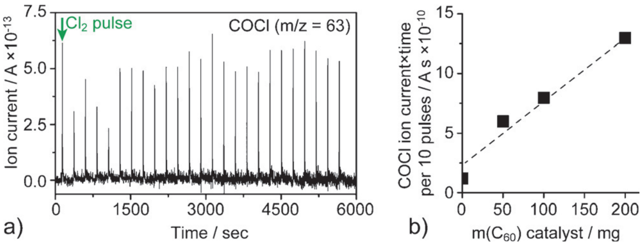

Figure 2. a) $COCl_2$ formation on applying Cl_2 pulses over solid C_{60} at 200 °C in 5% CO in He. b) Comparison of the $COCl_2$ formation in the presence of various amounts of C_{60} fullerene.

To probe the hypothesis that Cl_2 has to be weakly adsorbed to be successfully activated and converted into $COCl_2$, in situ Raman spectroscopy was used to study the interaction of Cl_2 with the C_{60} fullerene (Figure 3a). The pentagonal pinch mode A_{2g} at 1465 cm^{-1} was used to monitor the electronic environment of the carbon atoms.[8–10]

In the presence of Cl_2, the intensity of the A_{2g} band decreased, rapidly reaching a new equilibrium (Figure 3a). Purging with an inert gas reverted the spectral changes induced by Cl_2 addition. This demonstrates a reversible interaction between Cl_2 and C_{60} involving the formation of a $[C_{60}\cdots Cl_2]$ complex, presumably via a charge transfer from C_{60} to Cl_2.[11] Reduction of the spherical symmetry upon C−Cl bond formation eliminates the A_{2g} band and results in new Raman bands at 650–850 cm^{-1} (C−Cl vibration in $C_{60}Cl_{30}$; Supporting Information, Figure S3a). Combined Raman (Figure 3a) and elemental analysis (Supporting Information, Table S1) of the Cl_2 treated C_{60} further show that the $[C_{60}\cdots Cl_2]$ interaction has neither led to the formation of covalent C−Cl bonds nor significantly changed the symmetry of fullerene.

To characterize the reversibly adsorbed $[C_{60}\cdots Cl_2]$ species, ESR spectroscopy was used (Figure 3b). Neutral C_{60} has no unpaired electrons and is, therefore, ESR-inactive. However, in our studies an ESR signal at $g = 1.9864 \pm 0.01$ was observed for the nominally neutral C_{60} due to the presence of small amount (5.4×10^{17} spin g^{-1}) of paramagnetic defects generated during the synthesis procedure or the purification. The ESR line patterns indicate that these defects are delocalized over all the C atoms of the C_{60} cage, so that the contributions to the ESR line are dynamically averaged over all sites on C_{60}.[12] Upon Cl_2 exposure, a new strong signal was observed at $g_{eff} = 1.9928 \pm 0.02$ indicating the localized Cl_2 adsorption and formation of strong paramagnetic $[C_{60}\cdots Cl_2]$ charge-transfer complex.[12] The singlet line, an isotropic doublet without zero-field splitting peaks, indicates that the symmetry of the C_{60} fullerene cage was not changed by exohedral functionalization.

DFT calculations were performed to rationalize these experimental observations. Figure 4 shows the calculated reaction energy diagram for the activation of Cl_2 in the presence of C_{60}.

The activation of Cl_2 by C_{60} leading to C_{60}/Cl_2^S in the ground singlet state (S_0) proceeds with a prohibitively high-energy barrier (exceeding 400 kJ mol^{-1}, as estimated by relaxed potential energy scan calculations). Therefore, we

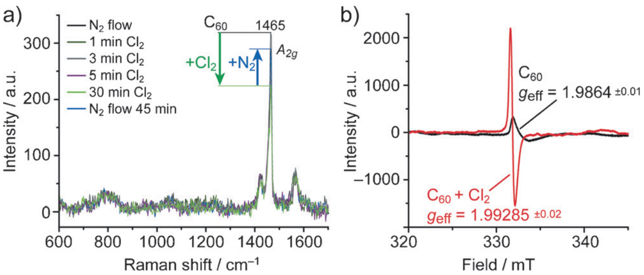

Figure 3. a) In situ Raman spectra of C_{60} contacted with Cl_2 at 40 °C. b) Comparison of the ESR spectra of C_{60} under inert conditions (black) and in a Cl_2 atmosphere (red) recorded at ambient temperature.

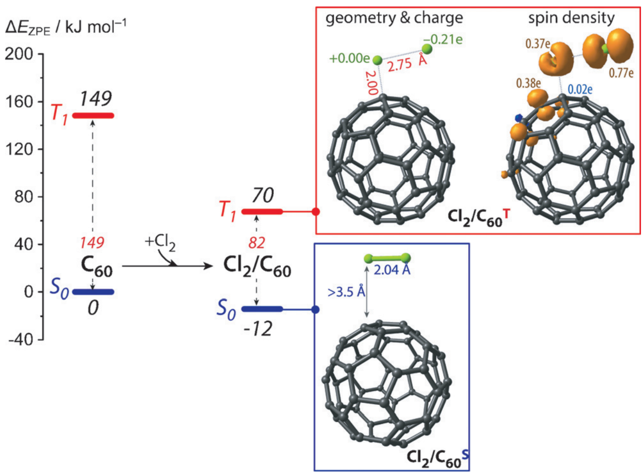

Figure 4. Reaction energy diagram and optimized structures (selected bond lengths are given in Å, Mulliken atomic charges and spin density are given for the open-shell Cl_2 adsorption complex Cl_2/C_{60}^T) of intermediates involved in Cl_2 adsorption and activation by C_{60} in the singlet (S_0) and triplet (T_1) electronic configurations.

conclude that a direct activation of Cl_2 on a C_{60} in the singlet state is not possible in the reaction space explored. Cl_2 activation becomes favorable when the reaction proceeds over the triplet excited potential energy surface. DFT-computed energy differences between the singlet (S_0) and triplet (T_1) electron configurations of C_{60} is 149 kJ mol^{-1}, that is, in excellent agreement with the reported experimental values (150–155 kJ mol^{-1}).[13,14] In the presence of Cl_2, the triplet electronic configuration (T_1, Figure 4, Cl_2/C_{60}^T) becomes strongly stabilized and is only 70 kJ mol^{-1} higher in energy than the respective ground state of a Cl_2 and C_{60} mixture. The T_1 adsorption complex Cl_2/C_{60}^T can be regarded as a biradical species featuring a Cl radical anion coupled with the $C_{60}Cl$ unit in which the spin density is delocalized, as shown in Figure 4. This is in line with the ESR spectra (Figure 3), showing the formation of Cl_2 radicals when Cl_2 is adsorbed on C_{60}. Such radical Cl_2/C_{60}^T species are hypothesized to be the key species for the catalytic conversion of CO to $COCl_2$. DFT calculations indicate a very favorable catalytic

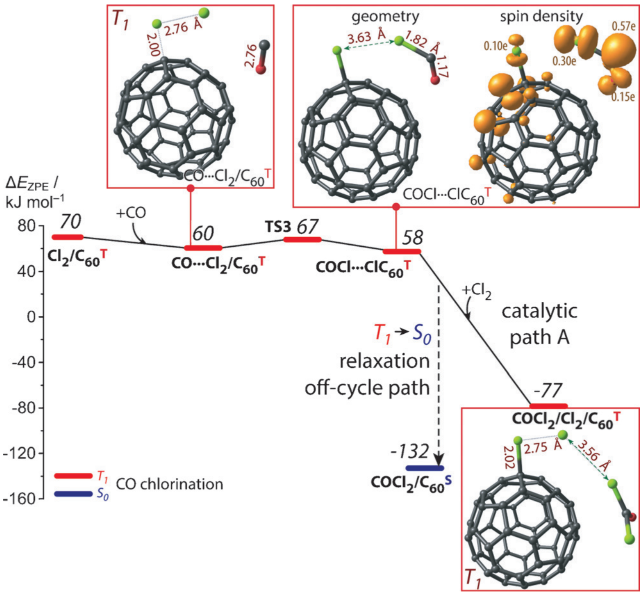

Figure 5. Reaction energy diagram and structures of key intermediates and transition states involved in phosgene synthesis over C_{60}.

path (Figure 5, Scheme 1). The cycle starts with the facile reaction ($E_{act} = 7$ kJ mol^{-1}) of CO with a Cl radical moiety of Cl_2/C_{60}^T yielding $COCl^•$ ($CO\cdots Cl_2/C_{60}^T \rightarrow COCl\cdots ClC_{60}^T$, Figure 5). The favorable path proceeds via a barrierless reaction of $COCl^•$ with another Cl_2 to yield $COCl_2$ (Figure 5) and regenerate Cl_2/C_{60}^T (Scheme 1, path A). However, the direct recombination of the $COCl^•$ and adjacent $Cl^•$ radicals (Scheme 1, path B) resulting in $COCl_2$ and transient C_{60}^T that is readily stabilized by Cl_2 to form Cl_2/C_{60}^T also cannot be completely ruled out. The off-cycle spin-crossing $T_1 \rightarrow S_0$ relaxation path (Figure 5) is less likely and would give a catalytic cycle with an apparent activation energy E_{act} over 70 kJ mol^{-1} needed for the transition to the active T_1 state (Figure 4). This is in a strong contrast to the observed barrier of 18 kJ mol^{-1} (Supporting Information, Table S2).

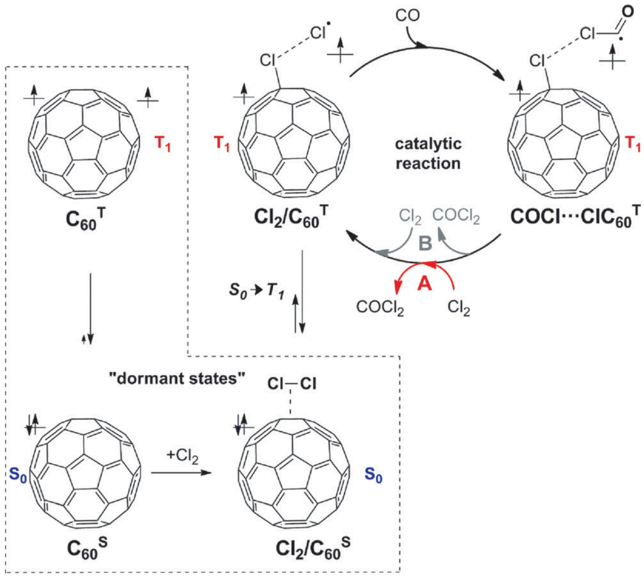

Scheme 1. Proposed mechanism for Cl_2/C_{60}^T catalyzed $COCl_2$ formation following an Eley–Rideal mechanism. The potentially dormant off-cycle species are shown in the dashed rectangle, while alternative paths for the regeneration of the catalytic species Cl_2/C_{60}^T are indicated as paths A and B.

The proposed reaction sequence is in line with the observed reaction order of one (Supporting Information, Table S2) in Cl_2 and CO. The apparent activation energy was significantly lower (18 kJ mol^{-1}) than that measured for an activated carbon catalyst (56 kJ mol^{-1}; Supporting Information, Table S2),[3] clearly indicating the subtle effect of the local environment of the active sites on the structure and energy of the transition state. At this point, we would like to stress that the proposed active site, the triplet [$Cl_2\cdots C_{60}$] will increase in concentration with temperature, as it lies 70 kJ mol^{-1} higher than the ground state of isolated C_{60} and Cl_2.

To independently probe the presence of radicals, [$C_{60}\cdots Cl_2$] was reacted with CH_4, which is known to be chlorinated by radical substitution. The reaction led to a mixture of CH_3Cl, CH_2Cl_2, and $CHCl_3$. In presence of C_{60} a five-fold rate increase compared to the non-catalytic thermal chlorination of CH_4 was observed at 200 °C (Figure 6) evidencing unequivocally the presence of surface-bound $Cl^•$ radicals.

Thus, combining ESR and Raman spectroscopic analysis and reactivity data, we conclude that a reversible surface bound radical [$C_{60}\cdots Cl_2$] species is formed, which reacts with CO to form $COCl_2$ and with CH_4 to form $CH_{4-n}Cl_n$. The $COCl_2$ formation is suggested to occur most likely via stepwise addition of Cl atoms. A second Cl_2 restitutes the reactive [$C_{60}\cdots Cl_2$] species, as the $COCl_2$ desorbs. The quite marked dependence of the Cl_2 reactions with carbon surfaces of various strain on the sp^2-hybridized carbons allows us to conclude that $COCl_2$ synthesis requires carbon catalysts with an intermediate strain to form a sufficient concentration of the critical reversibly bound radical [$C_{60}\cdots Cl_2$] species.

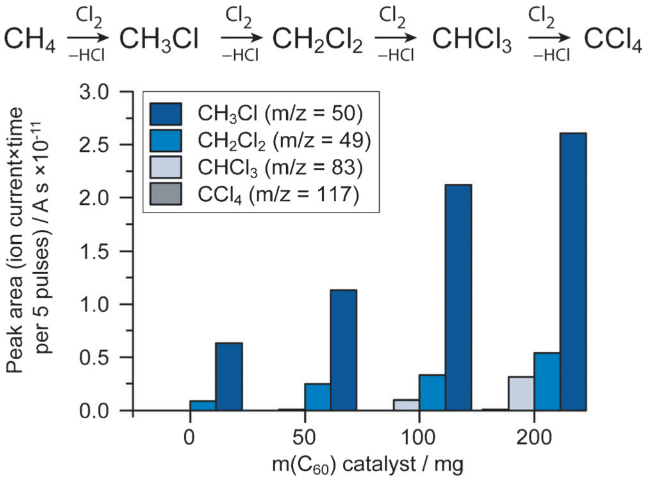

Figure 6. CH_4 chlorination in the absence (0 mg) and in the presence of variable amounts (50–200 mg) of C_{60} catalyst at 200 °C.

Experimental Section

C_{60} fullerenes (> 99.5 %) with a $S_{BET} < 5\ m^2 g^{-1}$ were purchased from Sigma–Aldrich. $C_{60}Cl_{30}$ was obtained from Nanofluor GmbH. TEM measurements were performed with a FEI TECNAI 20 electron microscope. The specific surface area and pore volume was determined by N_2 physisorption and Brunauer–Emmett–Teller (BET) using PMI automated Sorptomatic 1990 instrument. ESR spectra were recorded in perpendicular mode on an X-band Joel Jes Fa 200 spectrometer. The measurements were performed in a high-pressure quartz tube at 25 °C (9.45 GHz, 1 mW microwave power). The in situ Raman spectra were measured under isothermal conditions at 40 °C, and the samples were analyzed inside a quartz flow reactor; to maintain Cl_2 atmosphere, Cl_2 containing gas (25 % Cl_2 in He, Westfalen) was used. Prior to Cl_2 treatment the samples were activated at 150 °C for 1 h in N_2 flow (99.996 %, Westfalen). The Raman spectra at 514.5 nm (2.41 eV, Ar^+ laser) were taken with Renishaw spectrometer in a backscattering configuration every 43 s. To exclude the possibility of Raman spectral changes that are due to the laser irradiation, the blank test was performed under pure N_2 flow.

The catalytic activity of the carbon materials (≤ 80 μm particle size) was tested in a quartz pulse reactor (0.4 cm ID; Supporting Information, Figure S2). A six-port valve was used for the automated dosage of Cl_2. C_{60} was packed in a quartz tube reactor and thermally treated under inert conditions (150 °C, temperature ramp: 5 °C min^{-1}, 10 cm^3 s^{-1} He flow; 99.996 % He, Westfalen) during 1.0 h prior to measurements. Cl_2 pulses, 60 μL each, (Cl_2 > 99.996 %, Westfalen) were performed at intervals of 230 s, under atmospheric pressure. The gaseous products were characterized in situ by MS using a PFEIFFER OmniStar quadrupole mass spectrometer (QMS 200). For testing the reactivity of activated Cl_2 at 200 °C, pre-mixed 5 % CO and 5 % CH_4 in He (> 99.9 %, Westfalen) were used. The rate of $COCl_2$ formation was evaluated at a temperature range of 100–350 °C. The Cl_2 and $COCl_2$ containing gaseous residue was decomposed in two interconnected KOH containing bottles. An active carbon filter finally retained reactive components from the exiting stream.

DFT calculations were carried out using the B3LYP exchange-correlation functional as implemented in Gaussian 09 D.01.[15] Dispersion interactions were accounted with the D3 version of Grimme's dispersion with Becke–Johnson damping.[16] Full geometry optimizations were carried out using the 6-31G(d,p) basis set. The energies obtained at this step were further refined by single-point electronic energies computed using the larger TZVP basis set.[17] Reaction enthalpies were calculated by correcting the electronic energies for zero-point energies and finite temperature contributions calculated from the results of the normal mode analysis at 298.15 K and 1 atm. The accuracy of the selected method is confirmed by a close agreement between the computed and experimental energetics.

Acknowledgements

The research leading to these results has received funding from the European Community's Seventh Framework Program [FP7/2007–2013] under grant agreement no. NMP-LA-2010-245988 (INCAS). SurfSARA and NWO are acknowledged for providing access to supercomputer resources. The authors thank Dr. Christian Diedrich (BTS) and Dr. Weiyu Song (TU/e) for the discussions and their scientific support.

Keywords: chlorine · density functional calculations · fullerenes · phosgene · reaction mechanisms

How to cite: *Angew. Chem. Int. Ed.* **2016**, *55*, 1728–1732
Angew. Chem. **2016**, *128*, 1760–1764

[1] a) W. Schneider, W. Diller, *Phosgene*, *Ullmann's Encyclopedia of Industrial Chemistry*, Weinheim, Wiley-VCH **2005**; b) K. L. Dunlap, *Phosgene*, *Kirk-Othmer Encyclopedia of Chemical Technology*, John Wiley & Sons. Inc, Hoboken, New Jersey, **2010**, pp. 1–13; c) T. A. Ryan, E. A. Seddon, K. R. Seddon, C. Ryan, *Top. Inorg. Gen. Chem.* **1996**, *24*, 3–932; d) http://www.phosgenesafety.info, accessible after registration by the International Isocyanate Institute (III) in Manchester, GB; e) NIST Chemistry WebBook, accessed 16.04.**2015**, http://webbook.nist.gov.

[2] T. A. Ryan, E. A. Seddon, K. R. Seddon, C. Ryan, *Top. Inorg. Gen. Chem.* **1996**, *24*, 167–220.

[3] a) C. J. Mitchell, W. v. d. Borden, K. v. d. Velde, M. Smit, R. Scheringa, K. Ahrikaa, D. H. Jonesa, *Catal. Sci. Technol.* **2012**, *2*, 2109–2115; b) C. Potter, S. Baron, *Chem. Eng. Prog.* **1951**, *47*, 473–479; c) Z. Csűrös, R. Soós, I. Petneházy, G. T. Szabó, *Period. Polytech. Chem. Eng.* **1970**, *14*, 3–11; d) E. N. Shapatina, V. L. Kuchaev, M. I. Temkin, *Kinet. Catal.* **1977**, *18*, 968–972; e) E. N. Shapatina, V. L. Kuchaev, M. I. Temkin, *Kinet. Catal.* **1978**, *19*, 972–976.

[4] P. Serp, J. L. Figueiredo, *Carbon Materials for Catalysis*, John Wiley & Sons. Inc, Hoboken, New Jersey, **2009**.

[5] a) A. J. Stone, D. J. Wales, *Chem. Phys. Lett.* **1986**, *128*, 501–503; b) P. A. Thrower, *Chem. Phys. Carbon* **1969**, *5*, 217–320.

[6] J. Sloan, R. E. Dunin-Borkowski, J. L. Hutchison, K. S. Coleman, V. C. Williams, J. B. Claridge, A. P. E. York, C. Xu, S. R. Bailey, G. Brown, S. Friedrichs, M. L. H. Green, *Chem. Phys. Lett.* **2000**, *316*, 191–198.

[7] A. Goel, J. B. Howard, J. B. Vander Sande, *Carbon* **2004**, *42*, 1907–1915.

[8] F. N. Tebbe, J. Y. Becker, D. B. Chase, L. E. Firment, E. R. Holler, B. S. Malone, P. J. Krusic, E. Wassermann, *J. Am. Chem. Soc.* **1991**, *113*, 9900–9901.

[9] H. Kuzmany, M. Matus, B. Burger, J. Winter, *Adv. Mater.* **1994**, *6*, 731–745.

[10] D. S. Bethune, G. Meijer, W. C. Tang, H. J. Rosen, *Chem. Phys. Lett.* **1990**, *174*, 219–222.

[11] M. Kalbác, L. Kavan, M. Zukalová, L. Dunsch, *Small* **2007**, *3*, 1746–1752.

[12] a) N. G. Spitsina, M. V. Motyakin, I. V. Bashkin, K. P. Meletov, *J. Phys. Condens. Matter* **2002**, *14*, 11089–11092; b) A. I. Mikhaylov, V. A. Pakhomova, S. I. Kuzina, S. A. Baskakov, Y. M. Shul'ga, A. A. Volodin, V. E. Muradyan, *Nato Sci. Ser. II, Math.* **2007**, 155–158; c) L. Khachatryan, B. Dellinger, *Chemosphere* **2003**, *52*, 709–716; d) M. S. Dresselhaus, G. Dresselhaus,

P. C. Eklund, *Science of Fullerenes and Carbon Nanotubes: Their Properties and Applications.* Elsevier Science (USA), **1996**.
[13] M. G. Giuffreda, F. Negri, G. Orlandi, *J. Phys. Chem. A* **2001**, *105*, 9123–9129.
[14] R. Deng, M. Treat, O. Echt, K. Hansen, *J. Chem. Phys.* **2003**, *118*, 8563–8565.
[15] Gaussian 09 (Revision D.01), M. J. Frisch, Gaussian, Inc., Wallingford CT, **2009** (full reference is given in the Supporting Information).
[16] S. Grimme, S. Ehrlich, L. Goerigk, *J. Comput. Chem.* **2011**, *32*, 1456–1465.
[17] a) A. Schäfer, H. Horn, R. Ahlrichs, *J. Chem. Phys.* **1992**, *97*, 2571–2577; b) A. Schäfer, C. Huber, R. Ahlrichs, *J. Chem. Phys.* **1994**, *100*, 5829–5835.

Received: September 23, 2015
Published online: January 6, 2016

